NUMERICAL SIMULATION OF WEAR IN FIBER-REINFORCED COMPOSITE MATERIALS

Luis Rodríguez-Tembleque*[1]

[1] *Escuela Técnica Superior de Ingeniería, Universidad de Sevilla, Camino de los Descubrimientos s/n , Sevilla E-41092, Spain*
* *Corresponding Author: luisroteso@us.es*

Keywords: Anisotropic Wear, Composite Materials, Fiber Reinforced Plastics, Anisotropic Friction, Contact Mechanics

Abstract
This work presents a numerical methodology to compute wear in fiber-reinforced plastics (FRP) that are subjected to different frictional contact conditions. New anisotropic wear and friction constitutive laws are also proposed to take into account the influence of the fiber's orientation, on the tribological behavior of FRP. The formulation uses the Boundary Element Method (BEM) and/or the Finite Element Method (MEF) for computing the elastic influence coefficients, and contact operators over the augmented Lagrangian to enforce contact constraints. The new anisotropic wear and friction constitutive laws, and the proposed algorithm are applied to study some FRP materials. In these studies, it can be observed how the fiber orientation, or sliding orientation affect the normal and tangential contact compliance, as well as the contact traction distribution and wear evolution.

1. Introduction

Fiber-reinforced composite materials are being used increasingly for numerous applications in many different structural and mechanical components. Although fiber-reinforced plastics (FRP) are widely applied, there are not many numerical formulations that allow to analyze these polymer composites under different contact and wear conditions, especially due to the fact that particular contact and wear constitutive laws are required. Some experimental works have studied the significant influence of fiber orientation on the wear and frictional behavior of FRP composites. It has to be mentioned the works [1, 2, 3, 4, 5, 6], and more recently, [7]. These experimental works showed that the coefficient of friction depends on several factors including the combination of materials, the surface roughness or the fiber orientation (i.e. the largest coefficient of friction was obtained when the sliding was normal to the fiber orientation, while the lowest one was obtained when the fiber orientation was transverse) (see Fig. 1). Even considering a sliding direction on a plane parallel to the direction of fibers, [1] observed that the coefficient of friction sliding in parallel direction was smaller than in the transverse direction. In summary, there is experimental evidence that it is not only important to consider anisotropy of the bulk material properties but also the anisotropy of the tribological properties, using proper contact and wear constitutive laws, and efficient numerical formulations.

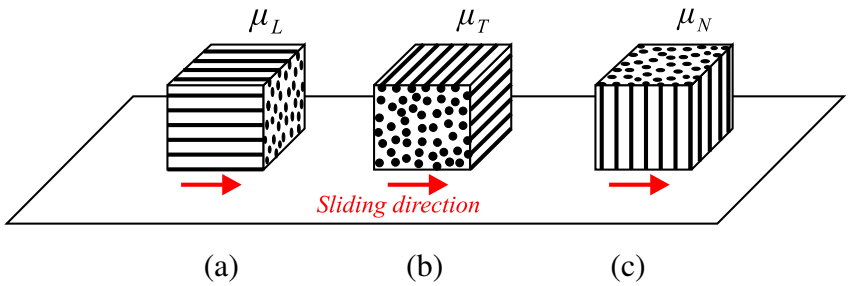

Figure 1. Schematic diagram of a unidirectional FRP indicating the sliding directions: (a) Longitudinal, (b) transverse, and (c) Normal ($\mu_L \leq \mu_T \leq \mu_N$).

2. Contact and wear constitutive laws for FRP

The contact problem between two linear anisotropic elastic bodies Ω^α, $\alpha = 1, 2$ with boundary $\partial\Omega^\alpha$ defined in the Cartesian coordinate system $\{x_i\}$ in $\mathbb{R}^3$ is considered. In order to know the relative position between both bodies at all times (τ), a gap variable is defined for the pair $I \equiv \{P^1, P^2\}$ of points ($P^\alpha \in \partial\Omega^\alpha, \alpha = 1, 2$), as $\mathbf{g} = \mathbf{B}^T(\mathbf{x}^2 - \mathbf{x}^1)$, where $\mathbf{x}^\alpha$ is the position of P^α at every instant ($\mathbf{x}^\alpha = \mathbf{X}^\alpha + \mathbf{u}_o^\alpha + \mathbf{u}^\alpha$), and matrix $\mathbf{B} = [\mathbf{e}_1|\mathbf{e}_2|\mathbf{n}]$ is a base change matrix defined in [8, 9, 10, 11, 12], which expresses the pair I gap in relation to the local orthonormal base (see Fig. 2(a)).

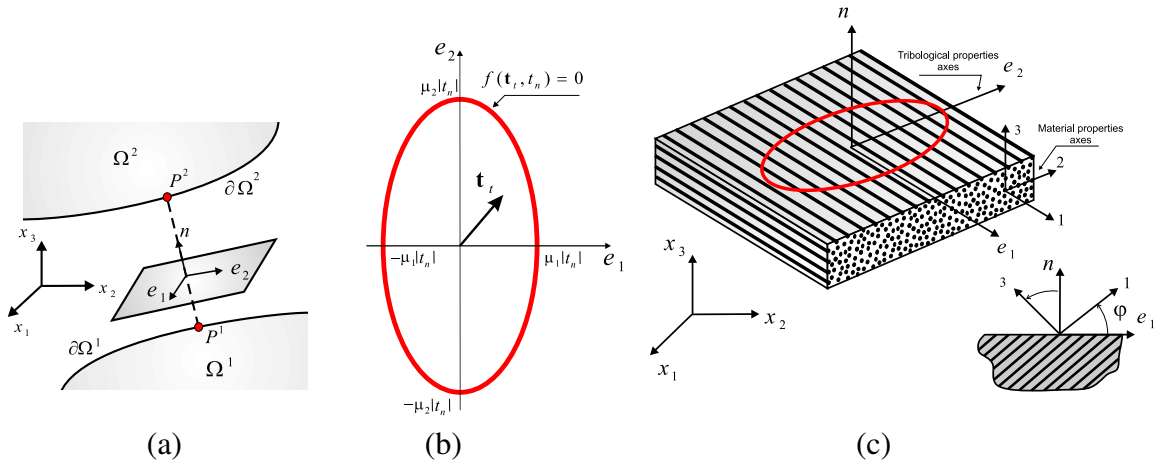

Figure 2. (a) Contact pair I of points $P^\alpha \in \Omega^\alpha$ ($\alpha = 1, 2$). (b) Elliptic friction law. (c) Orthotropic surface with parallel fibers.

The expression for the gap can be written as:

$$\mathbf{g} = \mathbf{g}_{go} + \mathbf{B}^T(\mathbf{u}^2 - \mathbf{u}^1) \tag{1}$$

where $\mathbf{g}_{go} = \mathbf{g}_g + \mathbf{g}_o$, $\mathbf{g}_g = \mathbf{B}^T(\mathbf{X}^2 - \mathbf{X}^1)$ being the *geometric gap* between two solids in the reference configuration, and $\mathbf{g}_o = \mathbf{B}^T(\mathbf{u}_o^2 - \mathbf{u}_o^1)$ the gap originated due to the *rigid body movements*. In this work, the reference configuration for each solid ($\mathbf{X}^\alpha$) that will be considered is the initial configuration (before applying load). Consequently, $\mathbf{g}_g$ may also be termed *initial geometric gap*. In the expression (1) two components can be identified: the normal gap, $g_n = g_{go,n} + u_n^2 - u_n^1$, and the tangential gap or *slip*, $\mathbf{g}_t = \mathbf{g}_{go,t} + \mathbf{u}_t^2 - \mathbf{u}_t^1$, being u_n^α and $\mathbf{u}_t^\alpha = [u_{t1}^\alpha, u_{t2}^\alpha]$ the normal and tangential components of the displacements.

2.1. Anisotropic contact law

The unilateral contact law involves two conditions in the *Contact Zone* (Γ_c): impenetrability and no cohesion. Therefore for each pair $I \equiv \{P^1, P^2\} \in \Gamma_c$: $g_n \geq 0$ and $t_n \leq 0$. The variable t_n is the normal contact traction defined as: $t_n = \mathbf{B}_n^T \mathbf{t}^1 = -\mathbf{B}_n^T \mathbf{t}^2$, where $\mathbf{t}^\alpha$ is the traction of point $P^\alpha \in \Gamma_c^\alpha$ expressed in the global system of reference, and $\mathbf{B}_n = [\mathbf{n}]$ is the third column of matrix $\mathbf{B} = [\mathbf{B}_t|\mathbf{B}_n]$. Tangential traction is defined as: $\mathbf{t}_t = \mathbf{B}_t^T \mathbf{t}^1 = -\mathbf{B}_t^T \mathbf{t}^2$. Finally, the variables g_n and t_n are complementary: $g_n\, t_n = 0$, so this set of relations may be summarized on Γ_c by the so-called Signorini conditions: $g_n \geq 0$, $t_n \leq 0$, $g_n\, t_n = 0$.

Friction constitutive laws for FRP can be accurately approximated by a convex elliptical friction cone, according to experimental works. The principal axes of the ellipse coincide with the orthotropic axes (Fig. 2(a)). The generic form of such anisotropic limit friction is given by

$$f(\mathbf{t}_t, t_n) = \|\mathbf{t}_t\|_\mu - |t_n| = 0 \tag{2}$$

where $\| \bullet \|_\mu$ denotes the elliptic norm $\|\mathbf{t}_t\|_\mu = \sqrt{(t_{e_1}/\mu_1)^2 + (t_{e_2}/\mu_2)^2}$, and the coefficients μ_1 and μ_2 are the principal friction coefficients in the directions $\{e_1, e_2\}$. Eq. 2 constitutes an ellipse whose principal axes are: $\mu_1|t_n|$ and $\mu_2|t_n|$ (see Fig. 2(b)). The classical isotropic Coulomb's friction criterion is recovered on Eq. 2 considering $\mu_1 = \mu_2 = \mu$. The allowable contact tractions $\mathbf{t}$ must satisfy: $f(\mathbf{t}_t, t_n) \leq 0$, defining an admissible convex region for $\mathbf{t}$: the *Friction Cone* ($\mathbb{C}_f$). An associated sliding rule is considered, so the sliding direction is given by the gradient to the friction cone and its magnitude by the factor λ: $\dot{g}_{e_1} = -\lambda \partial f/\partial t_{e_1}$ and $\dot{g}_{e_2} = -\lambda \partial f/\partial t_{e_2}$. To satisfy the complementarity relations: $f(\mathbf{t}_t, t_n) \leq 0$, $\lambda \geq 0$, $\lambda f(\mathbf{t}_t, t_n) = 0$, the expression for λ factor is: $\lambda = \|\dot{\mathbf{g}}_t\|_\mu^*$, where the norm $\| \bullet \|_\mu^*$ is dual of $\| \bullet \|_\mu$, so: $\|\dot{\mathbf{g}}_t\|_\mu^* = \sqrt{(\mu_1 \dot{g}_{e_1})^2 + (\mu_2 \dot{g}_{e_2})^2}$. Thus: $t_{e_1} = -\|\mathbf{t}_t\|_\mu \mu_1^2 \dot{g}_{e_1}/\|\dot{\mathbf{g}}_t\|_\mu^*$ and $t_{e_2} = -\|\mathbf{t}_t\|_\mu \mu_2^2 \dot{g}_{e_2}/\|\dot{\mathbf{g}}_t\|_\mu^*$. To sum up, the *unilateral contact condition* and the *elliptic friction law* defined for any pair $I \equiv \{P^1, P^2\} \in \Gamma_c$ of points in contact can be compiled as follows, according to their contact status: *no contact* ($t_n = 0$, $g_n \geq 0$ and $\mathbf{t}_t = \mathbf{0}$), *contact-adhesion* ($t_n \leq 0$, $g_n = 0$ and $\dot{\mathbf{g}}_t = \mathbf{0}$) and *contact-slip* ($t_n \leq 0$, $g_n = 0$ and $\mathbf{t}_t = -|t_n| \mathbb{M}^2 \dot{\mathbf{g}}_t / \|\dot{\mathbf{g}}_t\|_\mu^*$). The tangential slip velocity ($\dot{\mathbf{g}}_t$) is expressed at time τ_k as: $\dot{\mathbf{g}}_t \simeq \Delta \mathbf{g}_t / \Delta\tau$, where $\Delta \mathbf{g}_t = \mathbf{g}_t(\tau_k) - \mathbf{g}_t(\tau_{k-1})$ and $\Delta\tau = \tau_k - \tau_{k-1}$, according to a standard backward Euler scheme. $\mathbb{M}$ is a diagonal matrix:

$$\mathbb{M} = \begin{bmatrix} \mu_1 & 0 \\ 0 & \mu_2 \end{bmatrix} \tag{3}$$

whose coefficients are

$$\mu_1 = \mu_L + (\mu_N - \mu_L)\, \hat{\varphi} \qquad \mu_2 = \mu_T + (\mu_N - \mu_T)\, \hat{\varphi} \tag{4}$$

The expressions above establish a new constitutive friction law which can be applied to model friction in FRP. Parameter ($0 \leq \hat{\varphi} \leq 1$) is the nondimensional fiber orientation constant ($\hat{\varphi} = 2\varphi/\pi$), and ($0 \leq \varphi \leq \pi/2$) is the fiber orientation relative to direction $\mathbf{e}_1$ (see Fig. 2(c)).

The combined normal-tangential contact problem constraints can be formulated as [8, 9, 10]:

$$\mathbf{t} - \mathbb{P}_{\mathbb{C}_f}(\mathbf{t}^*) = \mathbf{0} \tag{5}$$

where the contact operator $\mathbb{P}_{\mathbb{C}_f}$ was defined as $\mathbb{P}_{\mathbb{C}_f}(\mathbf{t}^*) = \{\ \mathbb{P}_{\mathbb{E}_\rho}(\mathbf{t}_t^*) \quad \mathbb{P}_{\mathbb{R}_-}(t_n^*)\ \}^T$. The normal projection function, $\mathbb{P}_{\mathbb{R}_-}(\cdot)$, and the tangential projection function, $\mathbb{P}_{\mathbb{E}_\rho}$ were also defined in

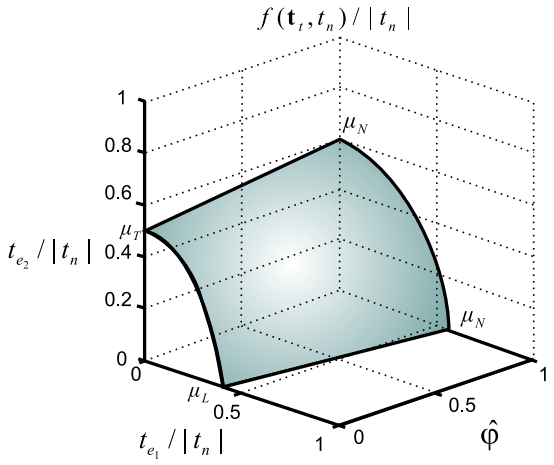

Figure 3. Friction surface ($f(\mathbf{t}_t, t_n)/|t_n|$) as a function of the fiber orientation $\hat{\varphi}$.

[8, 9, 10], as well as the augmented traction components $(\mathbf{t}^*)^T = [(\mathbf{t}_t^*)^T t_n^*]$: $\mathbf{t}_t^* = \mathbf{t}_t - r_t \mathbb{M}^2 \mathbf{g}_t$ and $t_n^* = t_n + r_n g_n$. r_n and r_t are the normal and tangential dimensional penalization parameters ($r_n \in \mathbb{R}^+, r_t \in \mathbb{R}^+$), respectively.

2.2. Anisotropic wear law

The wear constitutive law is based on [8, 9]. In these works, wear evolution can be expressed in the following wear rate form: $\dot{g}_w = i_w\, |t_n| \dot{D}_s$, g_w being the wear depth, $\dot{D}_s$ the tangential slip velocity module ($\dot{D}_s = \|\dot{\mathbf{g}}_t\|$), and i_w the dimensional wear coefficient or the specific wear rate. Assuming that the wear intensity i_w is a function of the sliding direction parameter α_v ($i_w = i_w(\alpha_v)$), wear velocity ($\dot{g}_w$) depends on the sliding direction. α_v is the measure of the oriented angle between the given direction ($\mathbf{e}_1$) and the sliding velocity direction. Let us consider an orthotropic wear law, $i_w(\alpha_v) = \sqrt{(i_1 \cos\alpha_v)^2 + (i_2 \sin\alpha_v)^2}$, where: $\cos\alpha_v = \dot{g}_{e_1}/\|\dot{\mathbf{g}}_t\|$, $\sin\alpha_v = \dot{g}_{e_2}/\|\dot{\mathbf{g}}_t\|$, and i_1 and i_2 are the principal intensity coefficients:

$$i_1 = i_L + (i_N - i_L)\,\hat{\varphi} \qquad i_2 = i_T + (i_N - i_T)\,\hat{\varphi} \tag{6}$$

whose expressions (6) establish a new constitutive wear law which can be applied to model friction in FRP. Finally, postulating the wear rate to be proportional to the friction dissipation energy makes $i_L = k\mu_L|t_n|$, $i_T = k\mu_T|t_n|$ and $i_N = k\mu_N|t_n|$, so they are related to friction coefficients through the wear factor k. So the wear intensity can be written as $i_w = \|\dot{\mathbf{g}}_t\|_i / \|\dot{\mathbf{g}}_t\|$, being $\|\dot{\mathbf{g}}_t\|_i = \sqrt{(i_1 \dot{g}_{e_1})^2 + (i_2 \dot{g}_{e_2})^2}$. Finally, the anisotropic wear law can be defined by

$$\dot{g}_w = |t_n|\, \|\dot{\mathbf{g}}_t\|_i \tag{7}$$

For quasi-static contact problems, wear depth defined on instant τ_k, is computed as

$$g_w = g_w(\tau_{k-1}) + |t_n|\, \|\Delta \mathbf{g}_t\|_i \tag{8}$$

$g_w(\tau_{k-1})$ being the wear depth value on instant τ_{k-1}. Due to the fact that the depth of removed material is computed for an instant τ_k, the normal contact gap (g_n) at the same time must be rewritten: $g_n = g_{go,n} + (u_n^2 - u_n^1) + g_w$.

3. Discrete equations for solids

3.1. Contact discrete variables and restrictions

The contact tractions ($\mathbf{t}_c$), the gap ($\mathbf{g}$), and the displacements ($\mathbf{u}^\alpha$, $\alpha = 1, 2$), are discretized over the contact interface (Γ_c). To that end, Γ_c is divided into N^f elemental surfaces (Γ_c^e). These elements (Γ_c^e) constitute a *contact frame*. The contact tractions are discretized over the contact frame as: $\mathbf{t}_c \simeq \hat{\mathbf{t}}_c = \sum_{i=1}^{N^f} \delta_{P_i} \boldsymbol{\lambda}_i$, where δ_{P_i} is the Dirac delta on each contact frame node i, and $\boldsymbol{\lambda}_i$ is the Lagrange multiplier on the node ($i = 1...N^f$). In the same way, the gap is approximated as $\mathbf{g} \simeq \hat{\mathbf{g}} = \sum_{i=1}^{N^f} \delta_{P_i} \mathbf{k}_i$. In the expression above, $\mathbf{k}_i$ is the nodal value. Therefore, taking into account the gap approximation, the discrete expression of Eq. 1 can be written as:

$$(\mathbf{k})_I = (\mathbf{k}_{go})_I + (\mathbf{d}^2)_I - (\mathbf{d}^1)_I, \tag{9}$$

for every contact pair I. In the expression above, $\mathbf{k}$ is the contact pairs gap vector and $\mathbf{k}_{go}$ the initial geometrical gap and translation vector. Finally, the contact restrictions (Eq. 5) for every contact pair I can be expressed as:

$$(\boldsymbol{\Lambda}_t)_I - \mathbb{P}_{\mathbb{E}_\rho}((\boldsymbol{\Lambda}_t^*)_I) = \mathbf{0} \qquad (\boldsymbol{\Lambda}_n)_I - \mathbb{P}_{\mathbb{R}_-}((\boldsymbol{\Lambda}_n^*)_I) = 0, \tag{10}$$

where augmented contact variables are defined as: $(\boldsymbol{\Lambda}_t^*)_I = (\boldsymbol{\Lambda}_t)_I - r_t \mathbb{M}^2 (\mathbf{k}_t)_I$ and $(\boldsymbol{\Lambda}_n^*)_I = (\boldsymbol{\Lambda}_n)_I + r_n (\mathbf{k}_n)_I$, and the value of ρ for the I pair: $\rho = |\mathbb{P}_{\mathbb{R}_-}((\boldsymbol{\Lambda}_{\boldsymbol{n}}^*)_I)|$.

3.2. FE-FE, BE-BE or FE-BE coupling equations

The formulation uses the BEM and/or the FEM for computing the elastic influence coefficients of every solid.The FE-FE, BE-BE or FE-BE contact system can be expressed, according to [8], as:

$$\begin{bmatrix} \mathbf{R}^1 & \mathbf{R}^2 & \mathbf{R}_\lambda & \mathbf{R}_g \end{bmatrix} \begin{Bmatrix} \mathbf{x}^1 \\ \mathbf{x}^2 \\ \boldsymbol{\Lambda} \\ \mathbf{k} \end{Bmatrix} = \bar{\mathbf{F}} \tag{11}$$

$\mathbf{x}^\alpha$ being the solid Ω^α ($\alpha = 1, 2$) unknowns, vector $\boldsymbol{\Lambda}$ represents the nodal contact tractions, and the matrices $\mathbf{R}^1$, $\mathbf{R}^2$, $\mathbf{R}_\lambda$ and $\mathbf{R}_g$, and vector $\bar{\mathbf{F}}$, the corresponding block matrices of these coupling systems as it was presented in [8].

3.3. Wear equations for contact problems

The wear depth for every instant can be discretized over the contact frame, as a function of the nodal values as $g_w^{(k)} \simeq \hat{g}_w^{(k)} = \tilde{\mathbf{N}} \mathbf{w}^e$, being $\tilde{\mathbf{N}}$ the shape functions matrix defined for the frame element Γ_c^e, and $\mathbf{w}^e$ the nodal wear depth vector of element Γ_c^e. Therefore, the discrete form of kinematic equation for I pair, at instant k, is

$$(\mathbf{k}^{(k)})_I = (\mathbf{k}_{go}^{(k)})_I + (\mathbf{d}^{2(k)})_I - (\mathbf{d}^{1(k)})_I + (\mathbf{C}_{g_n} \mathbf{w}^{(k)})_I \tag{12}$$

where $\mathbf{w}^{(k)}$ is a vector which contains the contact pairs wear depth, and matrix $\mathbf{C}_{g_n}$ is constituted using the $\mathbf{C}_g$ columns which affect the normal gap of contact pairs [8, 9]. The discrete expression of Eq. 8 can be written for I pair as

$$(\mathbf{w}^{(k)})_I = (\mathbf{w}^{(k-1)})_I + |(\boldsymbol{\Lambda}_n^{(k)})_I| \, \|(\mathbf{k}_t^k)_I - (\mathbf{k}_t^{(k-1)})_I\|_i \tag{13}$$

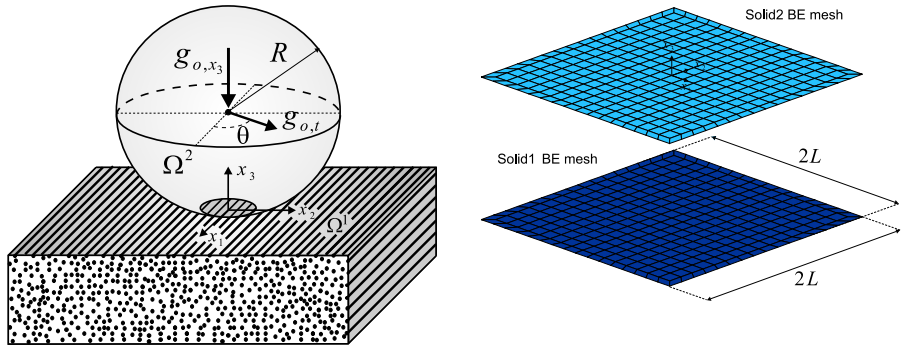

(a) (b)

Figure 4. (a) Sphere indentation over a FRP halfspace. (b) Boundary elements mesh details.

where $\mathbf{\Lambda}_n^{(k)}$ is a vector which contains the normal traction components of contact pairs at instant k.

4. Solution Scheme

The quasi-static wear contact problem equations set: Eq. 10 to Eq. 13, allow to compute the variables on instant or load step (k), $\mathbf{z}^{(k)} = [(\mathbf{x}^1)^T\ (\mathbf{x}^2)^T\ \mathbf{\Lambda}^T\ \mathbf{k}^T\ \mathbf{w}^T]^T$, when the variables on previous instant are known. In this work $\mathbf{z}^{(k)}$ is computed using the iterative Uzawa predictor-corrector scheme proposed in [8, 9, 10].

5. Numerical studies

This example presents a steel sphere of radius $R = 50\ mm$ indented on a carbon FRP half-space (see Fig. 4(a)). The sphere is subjected to a normal displacement $g_{o,x_3} = -0.02\ mm$ and a tangential translational displacement of module: $g_{o,t} = 0.008\ mm$, which forms an angle θ with axis x_1. The carbon FRP considered is IM7 Carbon/ 8551 − 7 with a volume fraction of 60 %, whose mechanical properties are: longitudinal Young modulus, E_1= 167.23 GPa, transverse Young modulus, E_2= E_3= 9.544 GPa, in-plane shear modulus, G_{12}= 5.292 GPa, transverse shear modulus ,G_{23}= 3.483 GPa, Poisson ratio ν_{12}= 0.272, and ν_{13}= 0.369. An anisotropic friction law is considered, being the friction coefficients: $\mu_L = 0.4$, $\mu_T = 0.5$ and $\mu_N = 0.55$. For simplicity, due to the contact half-width (a) will be much less than the radius (R), the solids are approximated by elastic half-spaces, each one discretized using linear quadrilateral boundary elements. Fig. 4(b) shows the meshes details, where the half-space characteristic dimension is $L = 1.2\ mm$. In this indentation problem, the influence of fiber orientation in the contact variables is considered. Figures 5(a) and (b), show the normal and tangential contact compliance variation with the fiber orientation, relative to the load for the fiber alignment $\varphi = 0^o$. For the normal load (Fig. 5(a)), the largest loads occur in the normal fiber orientation ($\varphi = 90^o$), and high differences can be observed for φ greater than 45^o. For the tangential contact compliance (5(b)), with $\theta = 0^o$, the variation relative to the load $Q(\varphi = 0)$ presents a different behavior. The largest discrepancies occur for a fiber orientation in the interval $[0^o, 45^o]$. For $\varphi = 90^o$, the tangential compliance is not affected by θ, because we recover the isotropic frictional behavior. Examining the Fig. 5(c), it is found that the variation of the orientation of the fibers has and

important effect on the magnitude of the normal and tangential contact tractions.

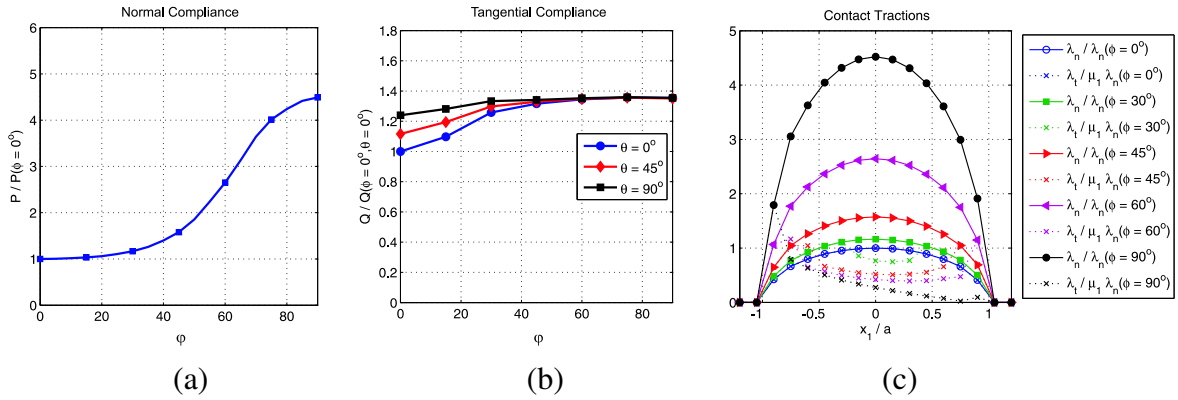

(a) (b) (c)

Figure 5. Normal (a) and tangential (b) contact compliance variation with the fiber orientation. (c) Influence of fiber orientation on the contact tractions distribution.

Wear coefficients: $i_L = 5 \times 10^{-10}\ MPa^{-1}$, $i_T = 6.25 \times 10^{-10}\ MPa^{-1}$ and $i_N = 6.875 \times 10^{-10}\ MPa^{-1}$, are considered to study a fretting wear problem under gross slip conditions. The wear volume evolutions after 100.000 cycles are presented in Fig.6(a), $g_{o,t} = 0.08\ mm$ being the applied tangential load amplitude. Fig.6(b) shows the influence of φ and θ on the resulting wear volume. Examining the Fig. 6(b), it is found that the variation of the orientation of the fibers has and important effect on the magnitude of wear, as well as the sliding direction for a fiber orientation in the interval $[0^o, 45^o]$.

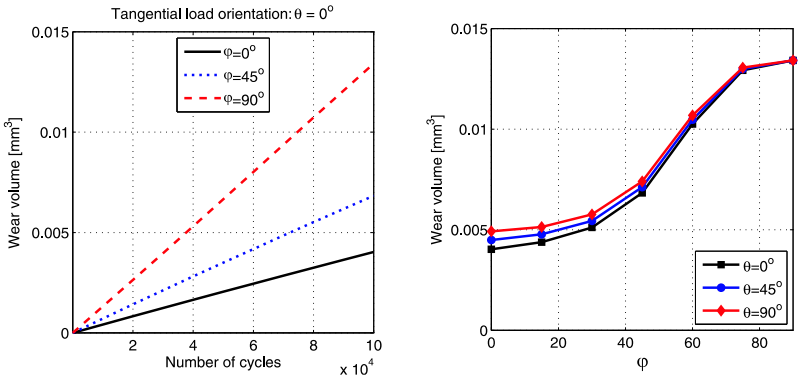

(a) (b)

Figure 6. (a) Wear volume evolution considering different fiber orientations. (b) Influence of the fiber orientation and the sliding direction in the resulting wear volume.

6. Summary and conclusions

This work presents new anisotropic wear and friction constitutive laws and its numerical implementation, to take into account the influence of the fiber orientation and the sliding direction, on the tribological behavior of FRP. Some examples are presented to show the importance of considering this new constitutive tribological properties. In other case, we could over- or underestimate wear and contact magnitudes and their distribution over the contact zone.

7. Acknowledgment.

The present research was supported by the was co-funded by the DGICYT of *Ministerio de Ciencia y Tecnología*, Spain, by project DPI2010-19331 which were co-funded by the European Regional Development Fund (ERDF) (Fondo Europeo de Desarrollo Regional, FEDER).

References

[1] N. Ohmae, K. Kobayashi and T. Tsukizoe. Characteristics of fretting of carbon fibre reinforced plastics. *Wear*, volume(29): 345–353, 1974.

[2] N.H. Sung and N.P. Suh. Effect of fiber orientation on friction and wear of fiber reinforced polymeric composites. *Wear*, volume(53): 129–141, 1979.

[3] T. Tsukizoe and N. Ohmae. Friction and wear of advanced composite materials. *Fibre Science and Technology*, volume(18): 265–286, 1983.

[4] M. Cirino, K. Friedrich, and R.B. Pipes. The effect of fiber orientation on the abrasive wear behavior of polymer composite materials. *Wear*, volume(121): 127–141, 1988.

[5] O. Jacobs, K. Friedrich, G. Marom, K. Schulte and H.D. Wagner. Fretting wear performance of glass-, carbon-, and aramid-fibre/ epoxy and peek composites. *Wear*, volume(135): 207–216, 1990.

[6] B. Vishwanath, A.P. Verma and V.S.K. Rao. Effect of reinforcement on friction and wear of fabric reinforced polymer composites. *Wear*, volume(167): 93–99, 1993.

[7] T. Larsen, T.L. Andersen, B. Thorning, A. Horsewell and M. Vigild. Fretting wear performance of glass-, carbon-, and aramid-fibre/ epoxy and peek composites. *Wear*, volume(262): 1013–1020, 2007.

[8] L. Rodríguez-Tembleque, R. Abascal and M. H. Aliabadi. Anisotropic wear framework for 3D contact and rolling problems. *Comput. Meth. Appl. Mech. Eng.*, volume(241): 1–19, 2012.

[9] L. Rodríguez-Tembleque, R. Abascal and M.H. Aliabadi. Anisotropic fretting wear simulation using the boundary element method. *CMES–Computer Modeling in Engineering and Sciences*, volum(87): 127–155, 2012.

[10] L. Rodríguez-Tembleque and R. Abascal. Fast FE-BEM algorithms for orthotropic frictional contact. *Int. J. Numer. Methods Eng.*, volume(94): 687–707, 2013.

[11] L. Rodríguez-Tembleque, F.C. Buroni, R. Abascal and A. Sáez. Analysis of FRP composites under frictional contact conditions. *Int. J. Solids Struct.*, volume(50): 3947–3959, 2013.

[12] L. Rodríguez-Tembleque, A. Sáez and F.C. Buroni. Numerical study of polymer composites in contact. *CMES–Computer Modeling in Engineering and Sciences*, volume(96): 131–158, 2013.